THE UNIVERSITY *of* EDINBURGH
School of Physics
and Astronomy

Senior Honours Project

RICH Test Beam Data Analysis

Alexander Thomson-Strong
March 2023

Abstract

In October 2022, data was taken from a series of test beams, designed to test fast electronics for a Ring-Imaging Cherenkov detector (RICH) as part of the ongoing LHCb upgrade II R&D. The aim is to add timing information to the two existing LHCb RICH detectors in preparation for the HL-LHC era. After correcting for a time walk, the time resolution as a function of detector bias was obtained. A minimum resolution of 300 $\pm$ 5 picoseconds was achieved. Pixel to pixel variations were investigated, and it was found that pixels near the edge of the detector perform less effectively. It was also observed that before the TWC, higher bias resulted in lower time resolution, but the TWC almost entirely compensated for this difference. Therefore, it is suggested that the detector can be operated at a lower HV, within the range studied, without a significant loss of performance.

Declaration

I declare that this project and report is my own work.

Signature: A Thomson - Strong Date: 30/03/2023

Supervisor: Dr. F. Oliva, Dr. S. Gambetta 10 Weeks

Contents

1 Introduction **3**
1.1 The LHCb Experiment . . . 3
1.2 Cherenkov Radiation . . . 3
1.3 RICH Detector Principles . . . 3
1.4 High Luminosity LHC . . . 4

2 Methods **6**
2.1 RICH Test-Beam . . . 6
2.2 Test-Beam Data . . . 7
2.3 Time Walk . . . 7
2.4 Time Walk Correction . . . 9
2.5 Time Resolution . . . 9

3 Results & Discussion **11**
3.1 Time Walk Correction . . . 11
3.2 Time Resolution . . . 11
3.3 TWC Efficiency vs Bias . . . 14
3.4 Pixel to Pixel Variation . . . 14

4 Summary & Conclusions **16**

5 Outlook **16**

A Appendices **20**

1 Introduction

1.1 The LHCb Experiment

The Large Hadron Collider (LHC) is a particle accelerator at the forefront of particle physics research. The LHCb is one of the major experiments at the LHC.

The LHCb began collecting data in 2009, with a focus on CP violation and rare decays of beauty and charm hadrons. It is a forward spectrometer, designed to detect particles produced in high energy proton-proton collisions [2].

The primary goal is to find indirect evidence of beyond the standard model physics through the observation of CP violation, and to provide insight into the apparent asymmetry between matter and antimatter in our universe [2][3].

High performance particle identification (PID) is a crucial component of the LHCb experiment. In the original LHCb RICH technical design report, it is stated that "meaningful CP-violation measurements are only possible if hadron identification is available" [4]. This is provided by two Ring-Imaging Cherenkov (RICH) detectors, RICH1 and RICH2. The LHCb RICH detectors combine measurements of particle momentum and emitted Cherenkov radiation to determine the mass of detected particles, and thus determine the species.

PID performance is evaluated based on the rate at which true kaons are identified as kaons, and the rate at which true pions are misidentified as other types of particle. During LHC run 2 [1], a kaon efficiency of 95% and pion misidentification of 10% was achieved over a momentum range of 2 to 100 GeV/c [5].

There are plans to increase the luminosity of the LHC by around an order of magnitude, the so-called high-luminosity LHC upgrade (HL-LHC)[6], which will allow for rare decay processes to be observed with greater statistics. Optimistically, new decays might also be observed for the first time.

This higher luminosity environment will be more challenging for PID [7], and therefore upgrades to the LHCb RICH system will be necessary to maintain the current PID performance.

1.2 Cherenkov Radiation

Cherenkov radiation is electromagnetic radiation which is emitted by a particle moving faster than the speed of light in the medium that it is travelling through.

When a charged particle moves through a medium, the particles within the medium become polarised, and they enter an excited state. Spherical wave-fronts are created when they de-excite back to the ground state. If the velocity of the charged particle, v_p, is greater than $\frac{c}{n}$, where c is the speed of light in a vacuum & n is the refractive index of the medium, constructive interference between wave-fronts creates a cone-shaped light signal with a characteristic angle, the Cherenkov angle θ_c [8].

It is can be inferred from figure 1 that the emission angle is given by equation 1

$$cos(\theta_c) = \frac{1}{n\beta} \tag{1}$$

where β is equal to $\frac{v_p}{c}$. This illustrates the ideal case, where there is no dispersion, meaning that the refractive index in independent of wavelength.

1.3 RICH Detector Principles

A RICH detector uses a measurement of the Cherenkov angle, and a measurement of the charged particle's momentum, provided

[1] From 2015 to 2018

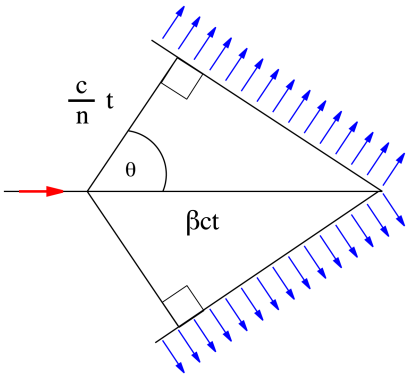

Figure 1: A charged particle moves from left to right in a medium with refractive index n. The particle moves with velocity v_p which is greater than $\frac{c}{n}$. Cherenkov radiation is emitted at the Cherenkov angle θ_c. This is the ideal case, where there is no dispersion. Figure taken from [1]

by a separate momentum spectrometer, to calculate a particle's mass and thus assign probabilities to different species of particle.

The principle of a RICH detector is to use a plane of photon detectors to image a ring shaped projection of the Cherekov light cone and reconstruct the Cherenkov angle. The geometry used by the LHCb RICH detectors was first described in [9]. The cones are reflected onto the detector surface by a spherical mirror. Knowing the radius of curvature of the mirror allows a measurement of the radius of the Cherenkov ring to be used to reconstruct θ_c, as shown in figure 2.

Reconstructing a ring-image involves combining multiple measurements of Cherenkov angle, which reduces the uncertainty.

The velocity of the charged particle is calculated from equation 1 From the velocity and momentum of a particle, its mass can be inferred.

1.4 High Luminosity LHC

Figure 3 shows the timeline for LHC operations (top) and an illustration of the proposed corresponding upgrades to the RICH detectors (bottom).

The HL-LHC project is a proposed upgrade to the LHC, to increase the maximum luminosity by around an order of magnitude after long shutdown 3 [6]. This would result in a greater frequency of particle collisions occurring, which should allow the properties of rare physical processes to be measured with reduced uncertainties.

This increase in luminosity would result in an increase in occupancy in each pixel of the RICH detectors, which makes PID much more difficult [7]. At high occupancy, it becomes increasingly difficult to resolve between different Cherenkov rings, as they will "generally overlap" [12].

Therefore, the LHCb collaboration is proposing upgrades to the LHCb sub detectors, including RICH1 and 2, to be able to cope with, and fully exploit the increased luminosity [13]. As well as a time resolution of less than 100ps, a reduction of pixel sizes is planned. Smaller pixel sizes will result in a decrease in the number of hits per pixel and improve the spatial resolution of the RICH detectors. These improvements should combine to allow the LHCb experiment to fully take advantage of the HL-LHC upgrade. Figure 3 illustrates these planned improvements, with coincident hits shown in the same colour. The two images on

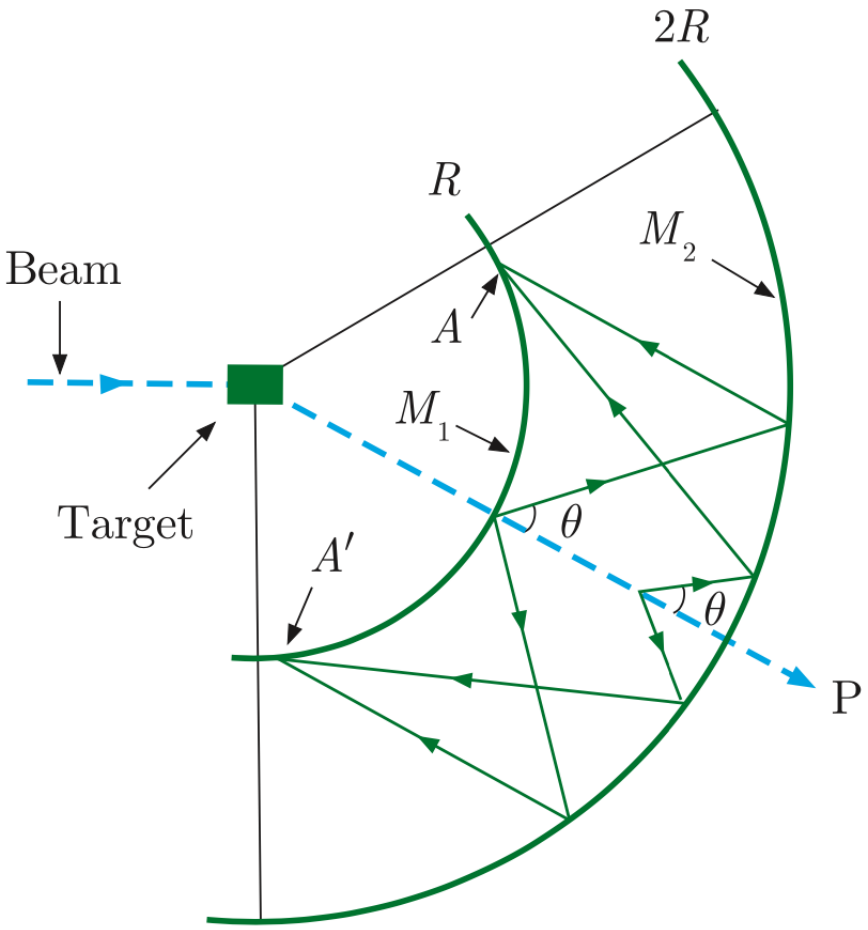

Figure 2: A diagram of a RICH detector, taken from [8] A charged particle beam moves from left to right. While moving through the radiator section, between R and 2R, $v_p > \frac{c}{n}$ and Cherenkov radiation is emitted. The radius of the ring-image is determined by the geometry of the system, and θ_c. M_2 is a mirror, which focuses the ring image onto the detector surface, M_1.

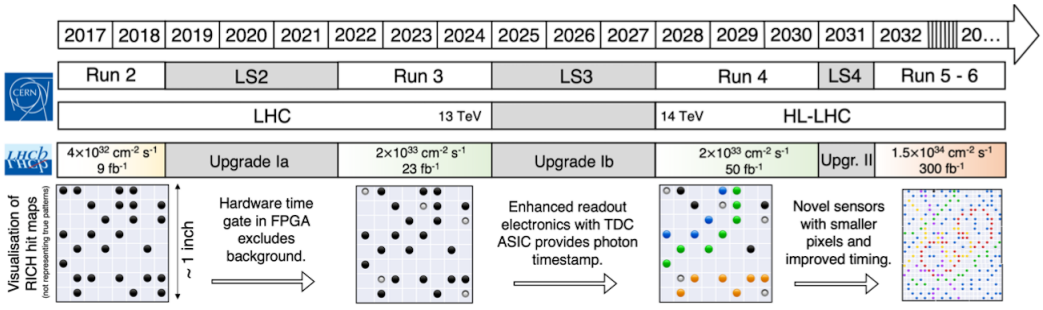

Figure 3: Figure taken from [10]. The top part of the figure shows the proposed timeline for the LHC and LHCb experiments. Below, is a graphical demonstration of the projected improvements that need to be made to the LHCb RICH detectors for the HL-LHC era. Note that the years associated with the timeline are not necessarily accurate after 2020, due to the disruption of the COVID-19 pandemic [11].

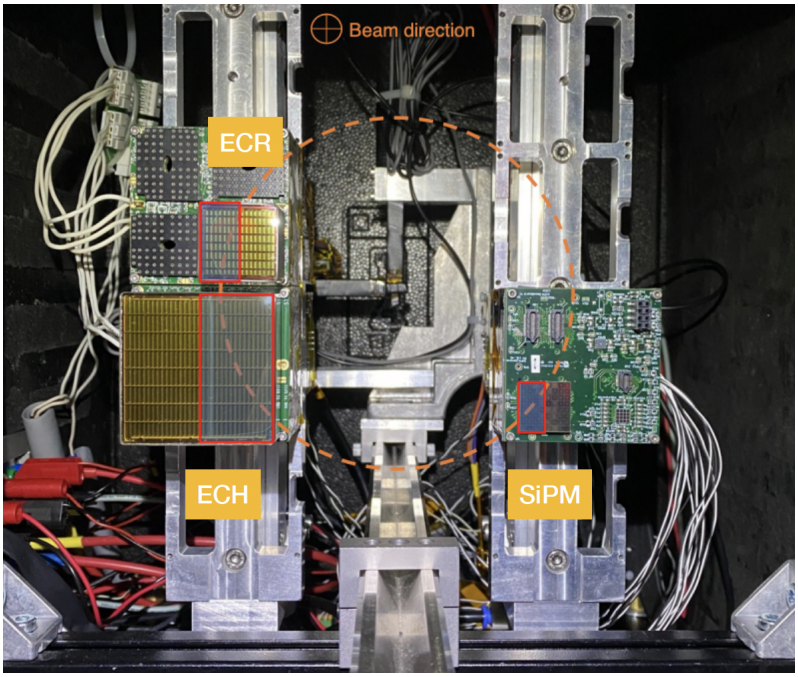

Figure 4: The set up for the October test-beams. Three different prototype photon detectors are labelled. The focus of this project was on the ECR, which is a Multi-anode Photo Multiplier Tube (MaPMT). A Cherenkov ring-image is superimposed in orange. Source: LHCb RICH internal material

the right have timing information included and this obviously makes it easier to resolve separate Cherenkov rings. As of right now, RICH1 and 2 have no timing information, and therefore can only resolve photons spatially. Thus, the addition of timing information to the detectors would represent a significant upgrade to their capabilities.

Currently, LHCb Upgrade II [13] is proposed to include applying fast electronics to LHCb RICH detectors. The goal of this would be to allow the existing RICH detectors to operate with a time resolution of less than 100 picoseconds, which is the predicted resolution that would be required to maintain the PID capability achieved in LHC run 2 [10].

As part of the ongoing R&D phase, prototypes have been tested in test beams at CERN's *Super Proton Synchrotron* (SPS), most recently in October 2022.

The aims of this project were to analyse the data from the October test beam experiments, to extract the time resolution of these fast electronics, and to evaluate the performance of the ECR detector 4.

2 Methods

2.1 RICH Test-Beam

In the SPS test-beam experiments, a particle beam is sent through a lens, which acts as the radiator to produce Cherenkov photons, and to focus the photons, which subsequently irradiate three separate prototype detectors. This experimental set-up is shown in figure 4. The detectors labelled ECR and ECH are both *Multi-anode Photo Multiplier Tubes* (MaPMT's) with pixel sizes of $2.8 \times 2.8\ mm^2$ and $5.6 \times 5.6\ mm^2$ respectively [14]. SiPM labels a Silicon Photo Multiplier detector.

In this dissertation, only the ECR is considered.

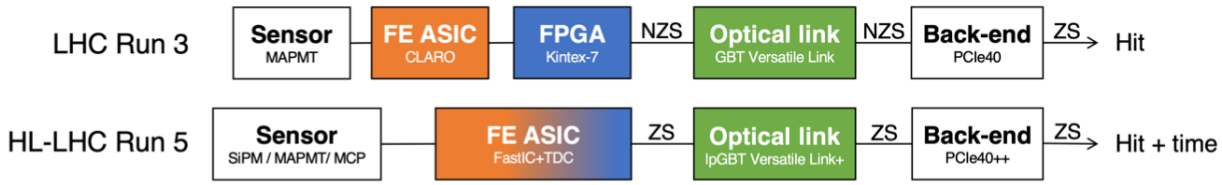

Figure 5: The electronic readout setup in LHC run 3 and planned for run 5. For run 5, timing information is added. Figure taken from [10].

The digital readout chain consists of a *Fast integrated circuit (FastIC)* and a *time-to-digital converter* (TDC) 5. A fixed threshold voltage discriminator is applied, which excludes low amplitude background signals from being recorded.

There are 4 FastICs, each with 8 channels that are connected to separate pixels of the MaPMT detectors. The FastICs record a digital signal, from which they can extract the time at which a signal crosses the threshold voltage - the *time of arrival* of that signal (ToA) and the total amount of time a signal is above the threshold - the *time over threshold* (ToT)[2] [15].

The TDC converts this timing information into digital bins, with an average width of 150 picoseconds. Calibration measurements were taken to allow these bin values to be translated into nanoseconds. The electronic readout set-up is visualised in figure 5.

A time-gate, which predicts when event photons [3] will arrive, acts like a "shutter" [10] to reduce background events at times when there shouldn't be any events recorded.

The detectors had an electric field bias applied, the amplitude of which sets the *gain* of the detector, which is defined as the number of photo-electrons which are produced for each incident photon [16]. The data collected from the test-beam campaign is divided into 5 runs, each with 32 pixels. Each run corresponded to a different *high voltage* bias (HV), with 800V, 850V, 900V, 950V, 1000V respectively.

Each run was completed in sequence, until $\approx$ 200k events were collected. The aim of this was to take data for each run under the same conditions.

The 32 pixels are arranged in space and numbered as shown in figure 6. The pixels connected to FastIC 5, inside the red rectangle, have a higher threshold applied.

2.2 Test-Beam Data

The data collected in the test-beam campaign was presented in the form of a ROOT file, and includes the ToA and ToT values, and their multiplicities for each run of the test-beam. The python package uproot4 [17] was used to analyse the available data. All coding was implemented in python and can be accessed at [18].

2.3 Time Walk

The threshold voltage is fixed for the duration of the test-beam, so no signal is recorded if the amplitude of a signal at a given time is less than a predetermined value. At the point where the analog signal exceeds the threshold voltage, the value of the digital output will jump from 0 to 1. This is referred to as the rising (or leading) edge of a signal. The point where the signal drops below the threshold is the falling (or

[2] see section 2.3

[3] as opposed to background photons.

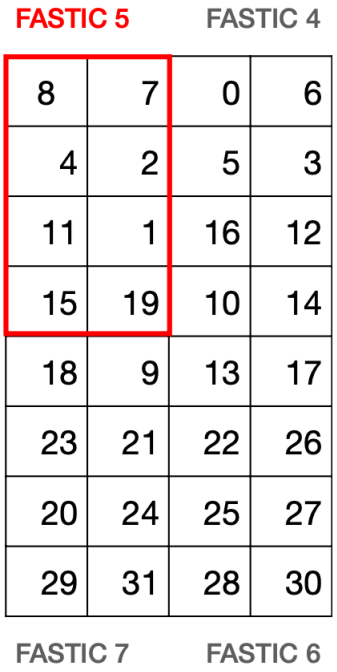

Figure 6: The channel labelling scheme for the test-beam campaign. FastIC 5, shown with the red rectangle, has a higher threshold voltage than FastIC 4, 6, 7.

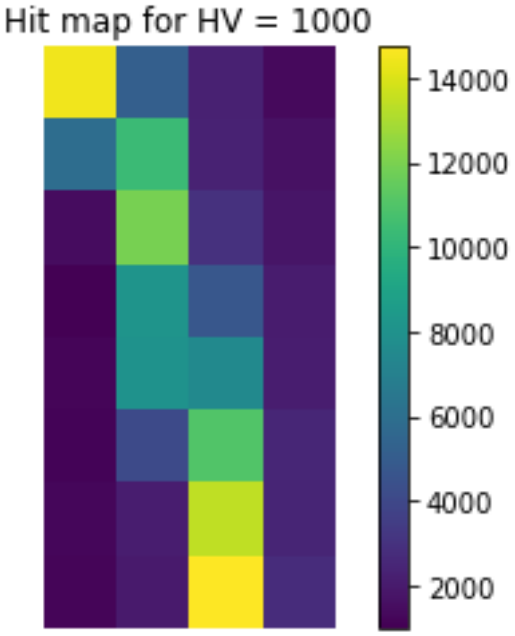

Figure 7: The hit map for the detector in the bias = 1000V run of the test-beam. The colour shows the number of hits in each pixel. The colour bar on the right shows the relationship between colour and number of hits. A fraction of the Cherenkov ring, including pixels 1, 2, 8, 13, 19, 22, 25 and 28, is clearly visible.

trailing) edge. The time that the rising edge of a signal occurs is the ToA, and the ToT is the time of the rising edge subtracted from the falling edge.

An analog signal with a large amplitude will surpass the fixed threshold earlier than a signal with a smaller amplitude. This results in an earlier ToA and a larger ToT. This behaviour is shown in figure 8. Thus, a greater ToT will clearly correspond to a greater amplitude. ToT can therefore be used as a measure of the amplitude of a digital signal, which is related to the number of photons.

This leads to digital signals which have ToA's offset by an amount referred to as a *time walk*. This difference has a systematic dependence on the ToT. Subtracting the predicted time walk, based on the ToT of each data point is referred to as a *time walk correction (TWC)*.

Applying a TWC removes the effect of this offset, such that the amplitude of a signal does not affect its measured arrival time. This is important for recognising signals which can be attributed to the same charged particle, and thus reconstructing Cherenkov ring-images.

Applying a TWC should also improve the time resolution of the RICH detector [19], which is an important consideration.

2.4 Time Walk Correction

The method described is adapted from [20]. A calibration curve is fitted to a 2D plot of mean ToA vs ToT, and then the predicted mean ToA is subtracted from the data at each ToT value.

The calibration curve for a time walk correction will have a characteristic shape with a plateau at large ToT. Pixels which have a large occupancy can include multiple plateaus, corresponding to signals where two or more photons arrive in the detector at the same time. This behaviour is seen in figure 10, where the distribution plateaus and then rises and plateaus again, although with a low frequency.

A successful fit can be achieved with functions of different forms. A physically justified function would be one that expresses the expected shape of the distribution. An example of this would be 2:

$$ToA = aToT^b + cToT + d \tag{2}$$

where a,b,c,d are parameters to be optimised to achieve the best fitting calibration curve.

This function works fine when you exclude the tails of the distribution, however in regions with high ToT, it performs poorly.

Instead, a polynomial function, with 6 degrees of freedom was chosen, which was found to reproduce the shape of the whole range of data more accurately than equation 2.

$$\begin{aligned} ToA = {} & aToT^5 + bToT^4 + cToT^3 + \\ & dToT^2 + eToT + f \end{aligned} \tag{3}$$

By applying a time walk correction, you can plot a 2D ToA vs ToT histogram for a number of signals and achieve a distribution such as in 12, where you can infer the amplitude from the ToT.

2.5 Time Resolution

The time resolution of a detector is the minimum amount of time between two signals that can be resolved from each other. By correcting for the time walk, we expect to achieve an improvement in the time resolution of the detector.

One way to estimate the time resolution of a pixel of the data [4] is to plot the ToA vs

[4] A systematic difference in the performance of different pixels, based on threshold and position was observed, see 3.4

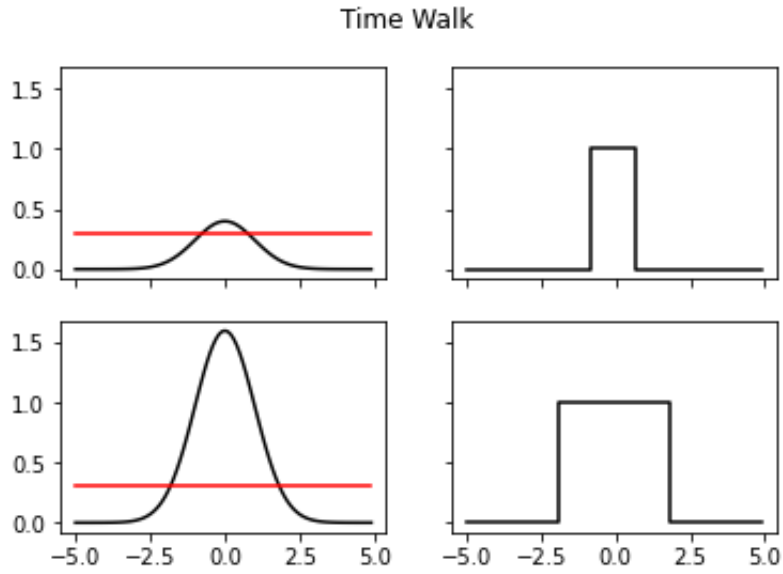

Figure 8: On the left, two analog signals are plotted. The red horizontal line shows a fixed voltage discriminator. On the right, the two signals are shown after being converted to digital. The top left signal has a lower amplitude than the bottom left signal. This results in the top right signal having a later rising edge and a lower ToT than the bottom right signal. This behaviour is referred to as a time walk.

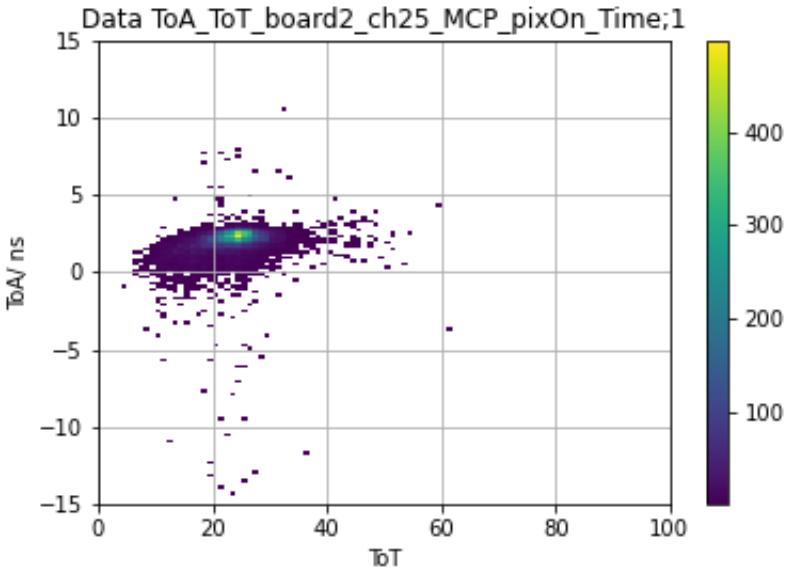

Figure 9: Two dimensional histogram showing the ToA vs ToT for pixel 25 in the 1000V detector bias run. The colour map shows the occupancy of each bin. ToA is displayed in nanoseconds and ToT is in TDC bins, with an average bin width of 150 picoseconds.

frequency of that pixel and fit a Gaussian function.

$$f(ToA) = \frac{1}{\sqrt{2\pi}\sigma} exp(-\frac{(ToA - \bar{ToA})^2}{2\sigma}) \quad (4)$$

The value of σ of this Gaussian function is then taken to be the estimate of time resolution.

Subsequent charged hadrons must arrive in the detector at times that are sufficiently separated for their Cherenkov rings to be resolved in time. This minimum amount of time will be set by the width of the distribution of ToA values 14, which justifies using σ as an estimate of the time resolution.

3 Results & Discussion

For each of the plots in this section, pixel 25 of the test-beam run using a 1000V bias was determined to be representative of the data. [18] contains the full set of plots produced for each pixel in each HV run of the test beam.

3.1 Time Walk Correction

Taking each pixel in a single run of the test beam individually and plotting a 2D histogram of ToA vs ToT, yields a plot like the one shown in 9. There is evidently a systematic dependence between ToA and ToT, which is characteristic of a time walk.

Taking vertical slices from the histogram that are the width of a single bin, the mean ToA for each ToT value was calculated and this data is illustrated in figure 10. A polynomial function was fit to this data using a weighted non-linear least-squares fit using the scipy.optimize.curve_fit method [21]. The weights were chosen to be the proportional uncertainty on the number of hits, N, in each slice, $\pm \sqrt{N}/N$.

Using the value of ToT for a particular data point, you can use the best-fitting polynomial that was found to estimate the value of the time walk and subtract it from the ToA. Still using just the mean ToA, and the corresponding ToT values, figure 11 is plotted as a validation plot. It is evident from inspection, that the mean ToA values are distributed around zero, with the majority of points within an error bar. This indicates that the TWC was performed correctly. Clearly, the TWC performs more poorly in the high ToT region, which is a consequence of the lower number of hits.

By applying this correction to the full data set, rather than just the mean, you achieve a similar transformation in the shape of the data. The time walk corrected ToA vs ToT 2D histogram is shown in figure 12.

3.2 Time Resolution

Again for pixel 25 with 1000V bias, the ToA distribution is shown before and after the TWC 13, and a separate Gaussian fit is applied to each of these distributions.

This is shown after the TWC is applied in figure 14. The optimised value of σ is 333 $\pm$ 4 picoseconds.

Fitting a similar Gaussian function to the frequency vs ToA plot without subtracting the time walk demonstrates the effect that the time walk correction has on the time resolution. The optimised value of σ for the uncorrected data is 345 $\pm$ 6 picoseconds. In this instance, this represents a 3.5 % improvement.

Before the TWC is applied, there is a prominent tail in the distribution. This is partially due to the time walk which causes the distribution to deviate from the

[5] Which can be verified by superimposing the distributions before and after the TWC, with their peaks aligned.

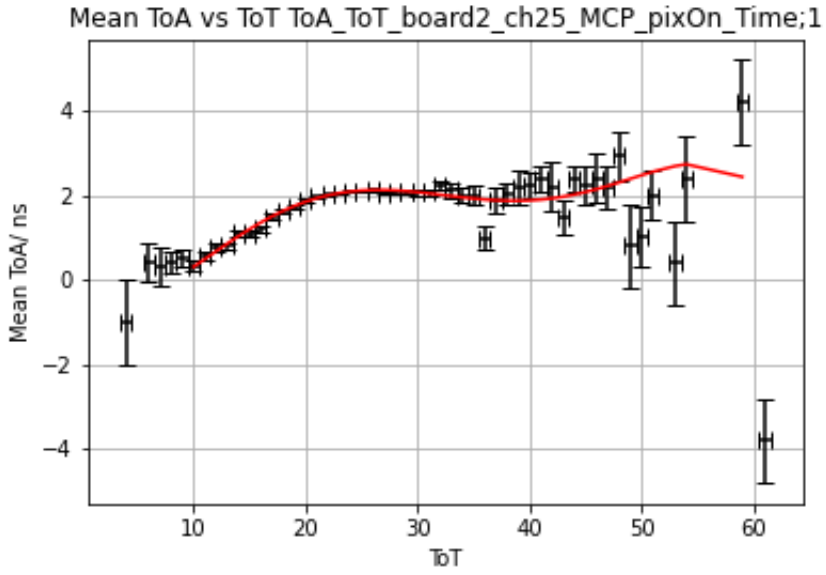

Figure 10: Mean ToA vs ToT for pixel 25 with bias = 1000V. The vertical error bars are the uncertainty due to the number of hits in each ToT slice. With N denoting the number of hits, the error is $\pm \sqrt{N}/N$. The horizontal error bars are $\pm$ half of the ToT bin width. The red line is equation 3 with parameters optimised by a non-linear least-squares fit. The vertical error bars were used as weights for the fit.

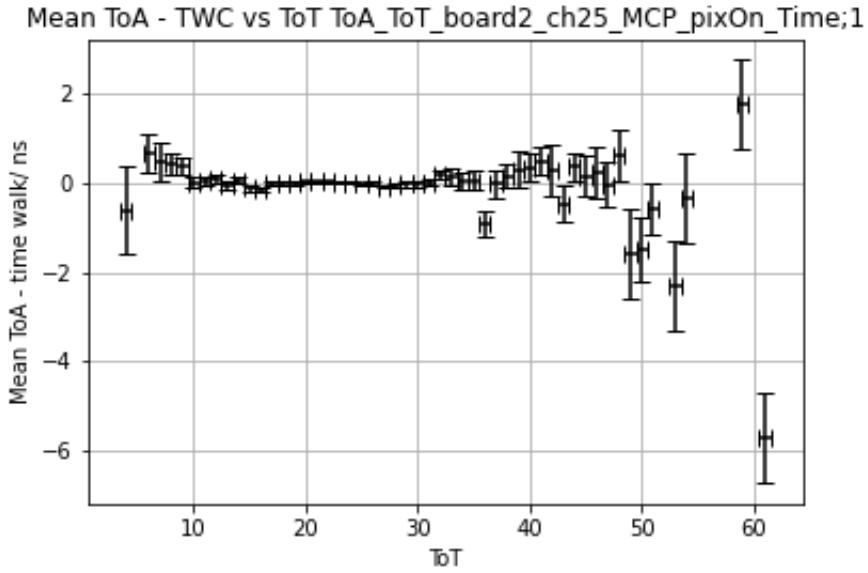

Figure 11: Mean ToA vs ToT with the time walk subtracted for pixel 25 with bias = 1000V. The vertical error bars are the uncertainty due to the number of hits in each ToT slice. With N denoting the number of hits, the error is $\pm \sqrt{N}/N$. The horizontal error bars are $\pm$ half of the ToT bin width.

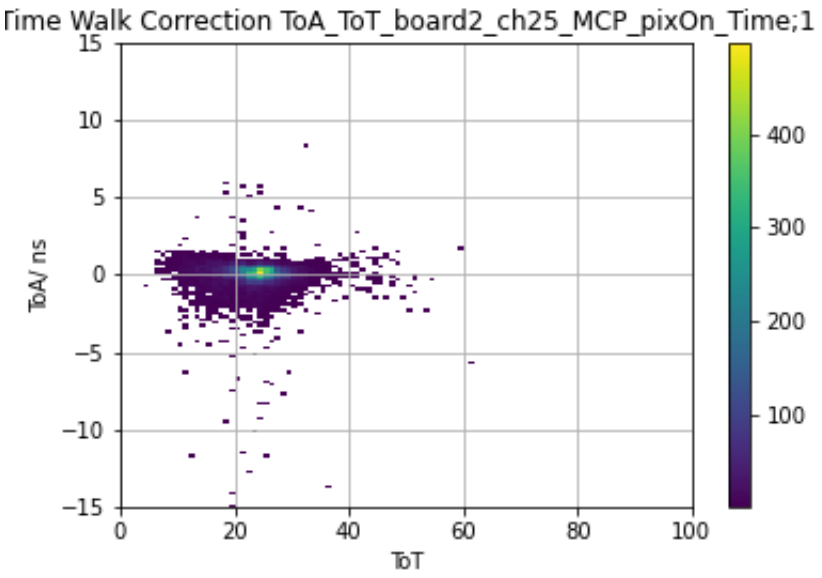

Figure 12: Two dimensional histogram showing the ToA vs ToT for pixel 25 in the 1000V detector bias run, after applying the TWC. The colour map shows the occupancy of each bin. ToA is displayed in nanoseconds and ToT is in TDC bins, with an average bin width of 150 picoseconds.

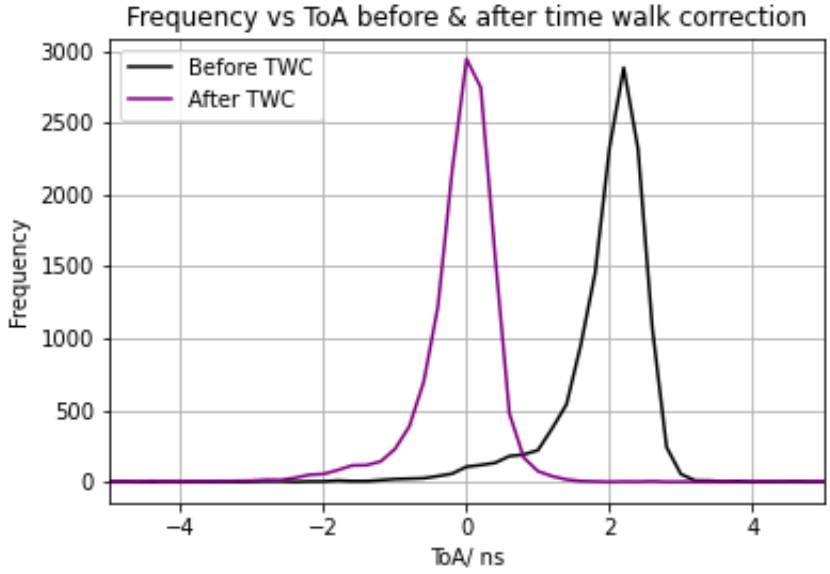

Figure 13: The distribution of ToA in pixel 25, with 1000V bias before and after the TWC.

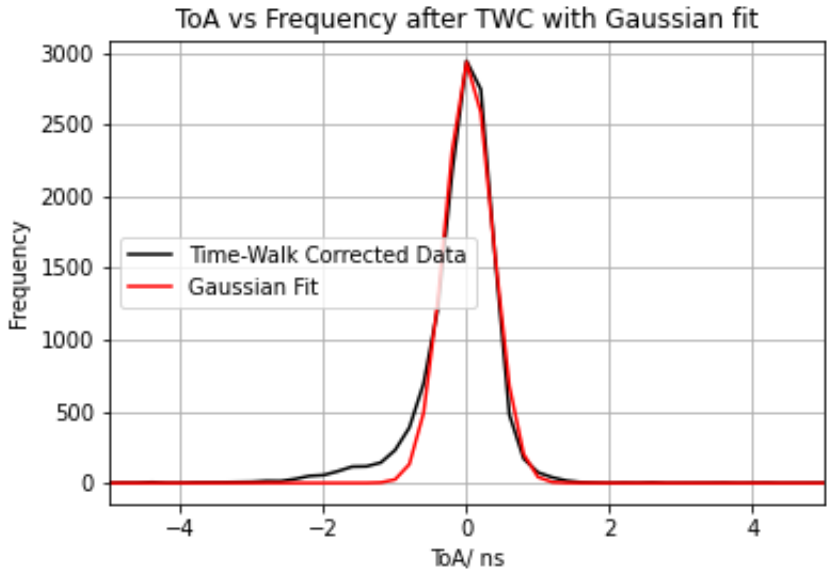

Figure 14: The distribution of ToA in pixel 25 after applying the TWC, with 1000V bias. Superimposed is a Gaussian fit

assumed Gaussian shape. After the TWC is applied, the tail is reduced [5] but a smaller tail remains. Processes that could contribute to this include back scattering, photons undergoing multiple reflections or dispersion.

3.3 TWC Efficiency vs Bias

Repeating this analysis for a single channel in each run allows you to plot the time walk corrected and uncorrected time resolutions against the bias voltage. This plot is shown in 15.

TWC efficiency is determined by:

$$E = 1 - \frac{\sigma_{after}}{\sigma_{before}} \tag{5}$$

where σ denotes the time resolution before and after the TWC.

Considering pixel 25, the efficiency of the TWC is very high for lower bias, and decreases rapidly as bias is increased. This is shown in figure 16. The TWC results in an improvement in the time resolution of 161 ps for 800V, which is greater than 30%, but a less than 5% improvement for 1000V. This same trend is observed in every pixel on the Cherenkov ring in the detector.

Although high bias voltages result in lower time resolutions before the TWC, applying the TWC eliminates this difference, and the time resolution becomes essentially flat against bias voltage. This is shown in figure 15, where it is obvious that the time resolution values are different by less than the uncertainty. This trend is also observed for each of the other pixels on the ring.

3.4 Pixel to Pixel Variation

Figure 17 shows the time resolution and channel number, for pixels on the Cherenkov ring with a 1000V bias. The same plots for the other HV runs are includes as appendices. Channel 13 was also on the ring, however there was an error in calibrating this channel in the experiment. Because of this error, the time resolution in this channel was anomalously high and thus is omitted.

Considering figures 6 and 17, it is clear

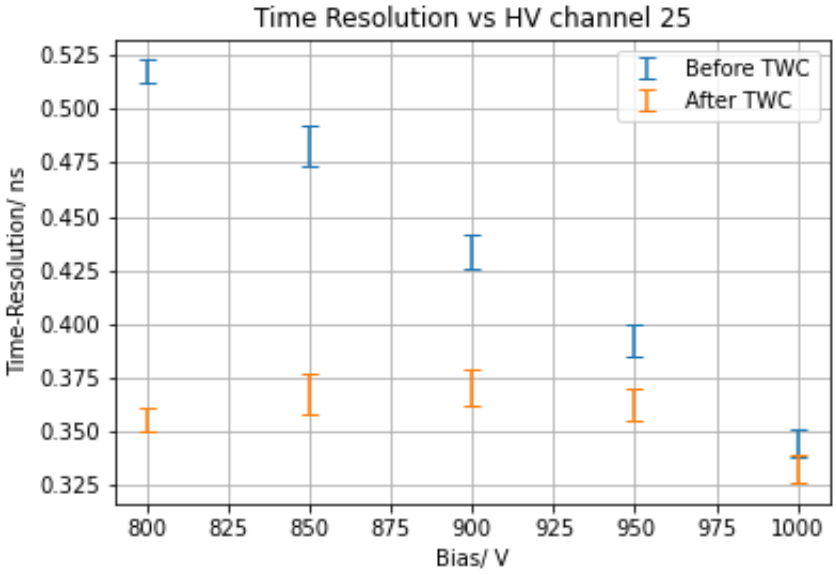

Figure 15: The time resolution before and after the TWC in channel 25, against the bias voltage applied to the detector. Before applying the TWC, increasing HV significantly improves time resolution. After applying the TWC, HV does not have a significant effect on the time resolution.

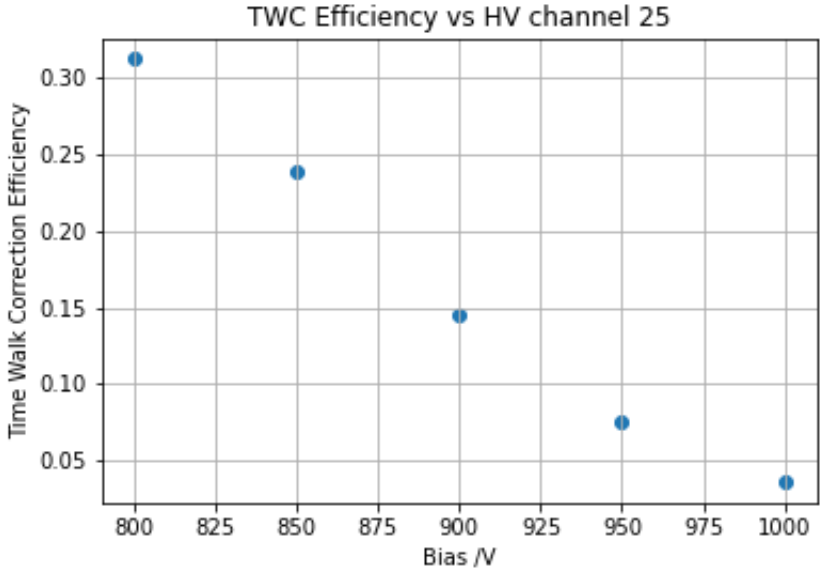

Figure 16: The efficiency of the time walk correction in channel 25, against the bias voltage applied to the detector. As HV increases, the TWC rapidly becomes less efficient. This trend is observed in every pixel.

that there is a systematic difference in time resolution due to pixel position.

Pixels 1, 2, 8 and 19 are all connected to FastIC 5, which has a higher threshold voltage than the other pixels. In order to isolate the effect of pixel position, pixels with the same threshold are compared.

In every run of the test-beam, the pixels with the highest time resolution were 8 (among higher threshold pixels) and 28 (lower threshold). These pixels are the only ones on the edge of the ECR, and on the Cherenkov ring.

The edges of the detector are where the noise levels are the highest, which increases the time resolution.

It appears that, when considering pixels that are away from the edge of the detector, the lowest time resolutions are achieved with the higher threshold voltage, although this might not necessarily be preferable. Lower bias voltage results in lower gain which, when combined with a high threshold results in a really low number of hits. Despite being on the ring, channel 1 has only 79 hits with 800V bias, compared to channel 25 which has 8222 hits in the same run.

4 Summary & Conclusions

In this project, a time walk correction method was developed in python, and applied to data collected in the October 2022 RICH test-beam at CERN SPS.

By fitting a calibration curve 3, the time walk was estimated for each ToT bin, and subtracted from the ToA values. This was applied to each pixel in the detector for each HV run.

For runs with a lower bias, the TWC resulted in a significant improvement in the time resolution. As the bias is increased, the efficiency of the TWC reduces, until the resolution before and after the TWC is the same to within the uncertainty. At sufficiently high bias, the time resolution before and after the TWC converge with each other.

Generally, you should expect a higher bias to improve the time resolution of a photon detector. However, here, the trend between bias and time resolution is essentially flat once the TWC is applied. Therefore, it appears that the MaPMT's can be operated at a lower HV without a significant loss of performance, within the HV range that was studied. As the detector ages, the gain will degrade, leading to fewer hits being recorded over time. To compensate for this, the HV is gradually increased. Beginning with a lower HV allows the HV to be increased by a greater amount as the detector ages. Therefore, beginning with a lower HV should allow the detectors to operate at a consistent performance for longer.

The time resolution on the Cherenkov ring was observed to be worse for pixels closer to the edge of the detector. This is a result of there being greater noise at the edges.

Generally, it appears that the time resolution is improved when using a higher threshold. This can be attributed to the exclusion of background noise. However, increasing the threshold is not necessarily advantageous, especially with low HV. A low gain and high threshold will result in really low statistics.

After excluding pixels in the detector that are not part of the Cherenkov ring, and those with low statistics (less than 1000 hits), the best time resolution found was 300 ± 5 picoseconds.

5 Outlook

The data analysis in this dissertation was applied only to the ECR detector. Using

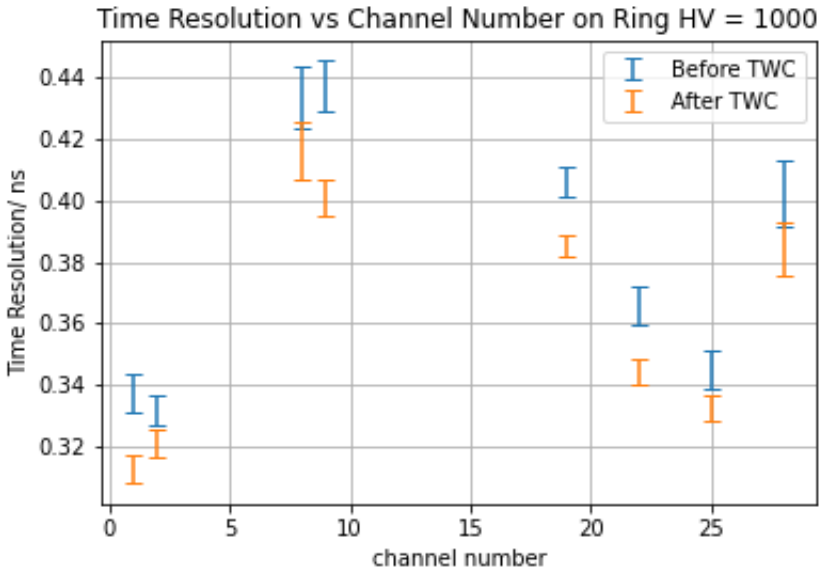

Figure 17: The time resolution in each channel on the Cherenkov ring for the 1000V bias run, before and after the TWC. The error bars show the uncertainty on σ returned by the Gaussian fit [21].

the same python code, the analysis can easily be reproduced for the ECH and SiPM detectors. This would enable the performances of the prototype detectors to be compared.

The success of the TWC in improving the time resolution of the detector is dependent of how well the calibration curve fits the ToA vs ToT distribution. This is sensitive to the form of the function used, the range of data used to perform the non-linear least-squares fit and its initial parameters, and the success of the noise reduction techniques used. Optimising these factors to maximise the improvement in the time resolution should be investigated further.

After excluding the tails of the data in figure 10, where the uncertainty is high, a calibration curve could be fit which would have an improved time resolution

In order to reduce the time resolution further, such that [6] the minimum time resolution of the system is achieved, multiple sources should be considered. A jitter, caused by noise and statistical fluctuations in the ToA should be investigated and compensated for [19]. Improvements in background signal reduction should also lead to an improvement in time resolution.

It would also be interesting to investigate the trend between time resolution and a wider range of voltages in a future test-beam. It was observed that after applying the TWC, the difference in time resolution between high and low bias runs is reduced significantly. If this trend can be observed at even lower HV than 800V, then it could be suggested that the detectors could be operated at an even lower bias without a substantial loss of performance. This would be beneficial for compensating the effects of aging. A problem with this is that reducing the HV will decrease the number of hits in the detector, and if coupled with a high threshold would lead to really low statistics. Below a certain HV, no signal would be reg-

[6] as close as possible to

istered in the detector.

While the time resolutions are significantly improved after applying the TWC, they are still significantly higher than the intrinsic resolution of the RICH system, of order 10ps [13], or the resolution required to maintain the current PID performance in the HL-LHC era.

The intrinsic resolution of the MaPMT's, which is of order 100 ps, is much greater than the intrinsic resolution of the RICH system. In the longer term, to reach a time resolution of less than 100 ps, a suitable candidate must be found to replace the MaPMT detectors.

Acknowledgements

I would like to thank my supervisor Federica Oliva for helping me throughout this project. Special thanks goes to my cat Jazz, for her invaluable emotional support.

References

1. Horvath, A. *File:cherenkov.svg* `https://commons.wikimedia.org/wiki/File:Cherenkov.svg`.
2. Alves, A. A. *et al.* The LHCB detector at the LHC. *Journal of Instrumentation* **3** (2008).
3. Matteuzzi, C. The lhcb rich system: Detector Performance. *Nuclear Instruments and Methods in Physics Research Section A: Accelerators, Spectrometers, Detectors and Associated Equipment* **766,** 245–249 (2014).
4. *RICH Technical Design Report - CERN* `https://cdsweb.cern.ch/record/494263/files/cer-2248787.pdf`.
5. Papanestis, A. & D'Ambrosio, C. Performance of the lhcb rich detectors during the LHC run II. *Nuclear Instruments and Methods in Physics Research Section A: Accelerators, Spectrometers, Detectors and Associated Equipment* **876,** 221–224 (2017).
6. Apollinari, G. *et al.* High-luminosity large hadron collider (HL-LHC). technical design report V. 0.1 (2017).
7. Keizer, F. & Wotton, S. *Sub-nanosecond Cherenkov photon detection for lhcb particle identification in high-occupancy conditions and semiconductor tracking for Muon Scattering tomography* PhD thesis (2019).
8. Martin, B. R. & Shaw, G. *Particle physics* (Wiley Blackwell, 2017).
9. Seguinot, J. & Ypsilantis, T. Photo-ionization and Cherenkov ring imaging. *Nuclear Instruments and Methods* **142,** 377–391 (1977).
10. Keizer, F. Novel photon timing techniques applied to the lhcb rich upgrade programme. *Journal of Physics: Conference Series* **2374,** 012074 (2022).
11. *New schedule for CERN's accelerators and experiments* `https://home.cern/news/news/accelerators/new-schedule-cerns-accelerators-and-experiments`.
12. Adinolfi, M. *et al.* Performance of the lhcb rich detector at the LHC. *The European Physical Journal C* **73** (2013).

13. LHCb Collaboration, CERN. *Framework TDR for the LHCb Upgrade II - Opportunities in flavour physics, and beyond, in the HL-LHC era* tech. rep. (CERN, Geneva, 2021). http://cds.cern.ch/record/2776420.

14. Bartolini, M. The upgrade of the lhcb rich detector. *Journal of Physics: Conference Series* **2374,** 012109 (2022).

15. Gómez, S. *et al.* Fastic: A fast integrated circuit for the readout of high performance detectors. *Journal of Instrumentation* **17** (2022).

16. Križan, P. Photon Detectors. *Handbook of Particle Detection and Imaging* (Jan. 2012).

17. *Uproot Documentation* https://uproot.readthedocs.io/en/latest/basic.html.

18. Thomson-Strong, A. R. *RICH Test Beam Data Analysis Code Repository* Feb. 2023. https://github.com/alexrt-s/RICH-Test-Beam-Data-Analysis.

19. https://www.ortec-online.com/-/media/ametekortec/other/fast-timing-discriminator-introduction.pdf?la=en.

20. Fiorini, M. *Proposal for a Time Walk Correction technique for the GTK EoC architecture* https://twiki.cern.ch/twiki/pub/Main/LinkToEOCDocs/20100713calibration.pdf.

21. *Scipy.optimize.curve_fit* https://docs.scipy.org/doc/scipy/reference/generated/scipy.optimize.curve_fit.html.

A Appendices

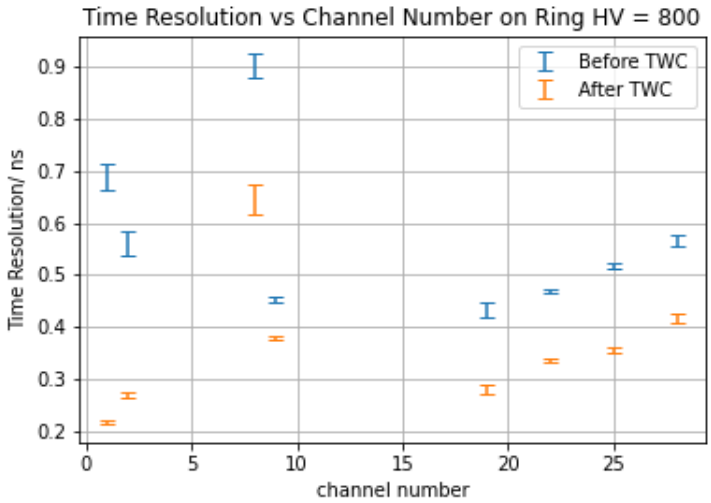

Figure 18: The time resolution in each channel on the Cherenkov ring for the 800V bias run, before and after the TWC. The error bars show the uncertainty on σ returned by the Gaussian fit [21].

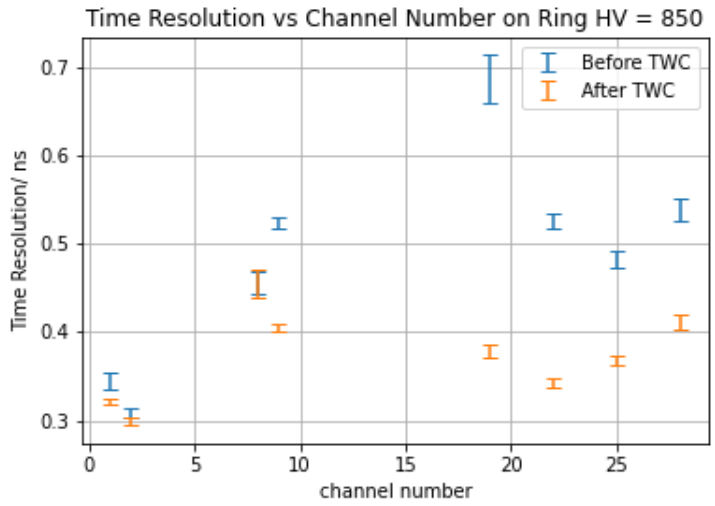

Figure 19: The time resolution in each channel on the Cherenkov ring for the 850V bias run, before and after the TWC. The error bars show the uncertainty on σ returned by the Gaussian fit [21].

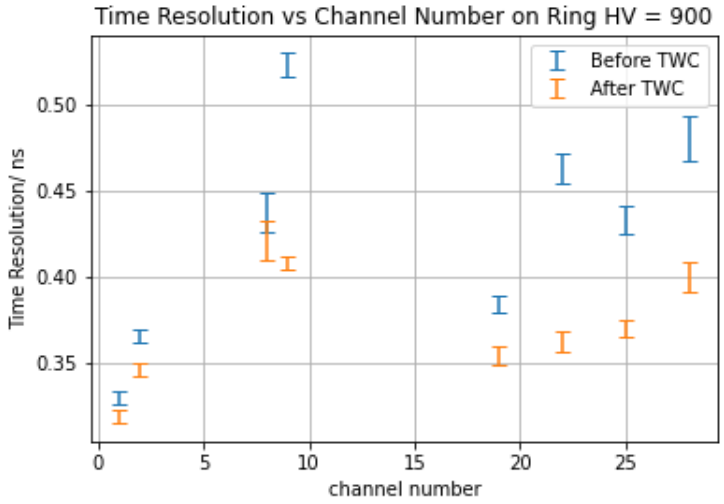

Figure 20: The time resolution in each channel on the Cherenkov ring for the 900V bias run, before and after the TWC. The error bars show the uncertainty on σ returned by the Gaussian fit [21].

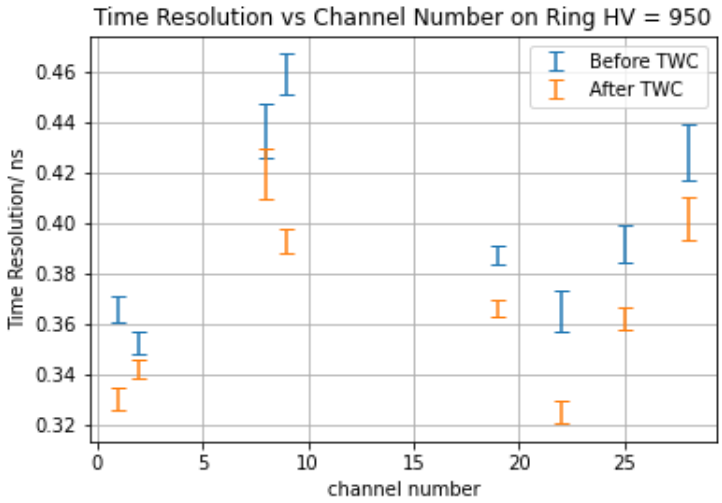

Figure 21: The time resolution in each channel on the Cherenkov ring for the 950V bias run, before and after the TWC. The error bars show the uncertainty on σ returned by the Gaussian fit [21].